ISSN 1061-933X, Colloid Journal, 2015, Vol. 77, No. 5, pp. 582–591. © Pleiades Publishing, Ltd., 2015.
Original Russian Text © A.E. Galashev, 2015, published in Kolloidnyi Zhurnal, 2015, Vol. 77, No. 5, pp. 593–602.

Mercury Droplet Formation on a Graphene Surface. Computer Experiment

A. E. Galashev

Institute of High Temperature Electrochemistry, Ural Branch, Russian Academy of Sciences, ul. Sof'i Kovalevskoi 22, Yekaterinburg, 620990 Russia
e-mail: galashev@ihte.uran.ru

Received January 27, 2015

Abstract—Molecular dynamics method has been employed to study rapid heating of a mercury film on graphene containing Stone–Wales defects. Hydrogenated edges of a graphene sheet withstand heating by 800 K. As the film contracts into a droplet, the horizontal component of the self-diffusion coefficient of Hg atoms monotonically decreases, while the vertical component passes through a deep minimum, which reflects the onset of droplet rising over the substrate. Droplet formation manifests itself as upward widening of the vertical density profile and an increase in the number of peaks in it. Therewith, the length of the radial distribution function of mercury substantially diminishes and the intensity of its first peak increases. Formation of the droplet leads to a decrease in the blunt contact angle. Temperature-related changes in graphene manifest themselves as a rise in the intensity of additional peaks in the angular distribution of the closest neighbors, oscillatory pattern of the stresses acting in its plane, and an almost linear growth of roughness.

DOI: 10.1134/S1061933X15040080

INTRODUCTION

Mercury absorption from smoke fumes has been studied with the use of X-ray absorption fine structure (XAFS) spectroscopy [1, 2]. XAFS spectra suggested that there is chemisorption of Hg on activated carbon. These data gave grounds to think that adsorption took place via halides, sulfides, and oxygen anions present on an activated-carbon surface. Moreover, chlorinated and bromated activated carbon was revealed with the use of X-ray absorption spectroscopy and X-ray photoelectron spectroscopy after exposure of carbon samples in smoke fumes containing Hg in an amount of 204 μg/m^3 [3]. Mercury was not found on the surface of activated carbon; however, Hg–Br and Hg–Cl complexes were present. This fact underlay the assumption that sites containing Cl and Br were formed on a carbon surface prior to the capture of Hg.

The mechanism of mercury binding by activated-carbon-based sorbents was studied in [4]. It was shown that, at low Hg concentrations, it was difficult to distinguish between the mechanisms of oxidation and adsorption. The difference between them gradually grew with Hg concentration and enhancement of Hg–Hg interaction. However, because of the close values of the bond energies in HgO, Hg_2Br_2, and $HgBr_2$, these surface-bound compounds were, as a rule, indistinguishable by photoelectron spectroscopy.

Liquid mercury does not wet graphite. Indeed, on highly ordered pyrolitic graphite, fresh mercury droplets have a contact angle of 152.5° [5]. As do any other liquid metals with surface tensions γ higher than 0.18 N/m, mercury does not wet carbon nanotubes [6]. The surface tension of mercury is 0.46 N/m. Nevertheless, wetting and filling of internal cavities of carbon nanotubes with mercury take place due to electrowetting [7]. The effect of electrostatic interactions on the sorption of hydrocarbons by water droplets (γ_{H_2O} = 0.0729 N/m) was shown in [8]. The mercury contact angle linearly increases with the curvature of carbon nanotube walls. Therefore, the internal surface of a nanotube has a higher phobicity with respect to mercury than the planar surface of graphene has [9]. Graphene wetting with mercury has not been studied.

Recently, graphene membranes have begun to be used in filters for separation of trace amounts of undesirable impurities [10, 11]. Repeated use of graphene in filters requires its nondestructive purification from adsorbed substances. Graphene may be purified from metals by irradiating with cluster beams of noble gases [12–15] or heating [16–19]. However, heating is reasonable to be used, when a metal has rather low boiling temperature T_b. Mercury seems to be a possible candidate for the use of this procedure. As a rule, ideal graphene is not destroyed upon heating to the boiling temperature of many metals, such as Al, Ni, or Cu, although its edges are damaged [16–18]. Graphene edges may be reinforced by hydrogenation. Graphene treated in this way withstands cluster bombardment even at a beam energy of 30 eV [20]. It is unclear how graphene with a high concentration of Stone–Wales defects will behave, because these defects are formed before its melting [21].

The goal of this work is to study the morphology and rapid-heating-induced variations in the physical properties of a mercury film on graphene with hydrogenated edges and a high concentration of Stone–Wales defects.

COMPUTER MODEL

Interatomic interactions in graphene were represented by the modified Tersoff many-particle potential [22]. This potential is based on the concept of bond order. Potential energy between two adjacent atoms i and j is described as follows:

$$V_{ij} = f_C(r_{ij})\left[A\exp(-\lambda^{(1)}r_{ij}) - Bb_{ij}\exp(-\lambda^{(2)}r_{ij})\right],$$

$$f_C(r_{ij}) = \begin{cases} 1, \\ \frac{1}{2} + \frac{1}{2}\cos\left[\pi\left(r_{ij} - R^{(1)}\right)\Big/\left(R^{(2)} - R^{(1)}\right)\right], \\ 0, \end{cases}$$

$$\begin{gathered} r_{ij} < R^{(1)} \\ R^{(1)} < r_{ij} < R^{(2)}, \\ r_{ij} > R^{(2)}, \end{gathered}$$

where b_{ij} is the many-particle bond order parameter that describes the generation of the energy of bond formation (attractive component V_{ij}) at a local atomic arrangement due to the presence of other neighboring atoms. Potential energy is a many-particle function of the positions of atoms i, j, and k; it is determined by the following parameters:

$$b_{ij} = (1 + \beta^n \xi_{ij}^{n_i})^{-1/(2n)},$$

$$\xi_{ij} = \sum_{k\neq i,j} f_C(r_{ij})g(\theta_{ijk}),$$

$$g(\theta_{ijk}) = 1 + \frac{c^2}{d^2} - \frac{c^2}{\left[d^2 + (h - \cos\theta_{ijk})^2\right]},$$

where ξ is the effective coordination number and $g(\theta_{ijk})$ is a function of the angle between $\mathbf{r}_{ij}$ and $\mathbf{r}_{ik}$, this is function stabilizing the tetrahedral structure.

We enlarged the distance of the covalent bonding to 0.23 nm and introduced additional weak attraction at $r > 0.23$ nm, with this attraction being specified by the Lenard-Jones (LJ) potential with parameters taken from [23]. The resulting rotational moment was eliminated in each site of a graphene sheet by excluding the rotational component of the force generated by the atoms of adjacent sites. The analytical form of the local rotational interaction potential had been given in [23].

In this work, the Hg–Hg interactions were determined with the use of the potential proposed by Silver and Goldman (the SG potential) [24]:

$$V_{SG}(r) = \exp(\alpha - \beta r - \gamma r^2) - f_c(r)\left(\sum_{n=3}^{5}\frac{C_{2n}}{r^{2n}}\right),$$

where

$$f_c(r) = \begin{cases} \exp\left[-(1.28r_c/r - 1)^2\right], & r < 1.28r_c, \\ 1.0 & r \geq 1.28r_c. \end{cases}$$

The parameters of the SG potential were presented in [24].

In addition, the calculations were repeated with the use of the Schwerdfeger (Sch) potential, which also adequately reproduces the main properties of mercury, such as melting temperature and density of liquid Hg. The Sch potential is based on ab initio calculations and has the following form [25]:

$$V_{Sch}(r) = U_{Sch}(\lambda r) = \sum_{j=3}^{9} a_2^* r^{-2j},$$

where U_{Sch} is the original Schwerdfeger potential for mercury dimer, $\lambda = 1.167$ is used for fitting to the density of liquid Hg at $T = 300$ K, and parameters a_{2j}^* have been given in [25].

The mercury–carbon and xenon–xenon interactions were specified by the LJ potential [25–27].

Defects substantially enhance metal adhesion to graphene. The Stone–Wales defects are among the most common defects in graphene (joined rings composed of five and seven carbon atoms). The graphene sheet used for mercury deposition had six such defects almost uniformly distributed over its area. Graphene edges were reinforced by hydrogenation. The CH groups formed on sheet edges were simulated using the single-atom scheme [28]. The C–CH and CH–CH interactions were described by the LJ potential [28]. The partial functionalization of graphene by the attachment of hydrogen atoms to its edges stabilizes the structure without an increase the interatomic distances and the creation of a roughness all over its surface.

A mercury film was formed on graphene by a separate molecular-dynamic (MD) calculation in two stages. At the first stage, Hg atoms were placed over the centers of nonadjacent cells of graphene in a manner such that the distance between Hg and C atoms was equal to 2.30 Å, as calculated in accordance with the density functional theory [4]. Additional 51 Hg atoms were deposited in a random manner onto this loose mercury film composed of 49 Hg atoms. The system consisting of 100 Hg atoms and 406 C atoms was then equilibrated over 10^6 time steps of MD calculation ($\Delta t = 0.2$ fs). The motion equations were numerically solved using the Verlet algorithm [29]. In addition, the

system thus obtained was stepwise heated, with the temperature being increased by 100 K relative to a previous state and the final configuration of a previous calculation being used as an initial one for a new state. The calculation at each temperature lasted 10^6 time steps.

The temperature in the system was maintained according to the Berendsen scheme with binding constant $\tau = 4$ fs [30]. At each time step, velocities v were scaled as follows:

$$v = \lambda v, \quad \lambda = \left[1 + \frac{\Delta t}{\tau}\left(\frac{T_0}{T} - 1\right)\right]^{1/2},$$

where λ is the scale factor, T_0 is the preset temperature (300 K), and T is the current temperature.

The self-diffusion coefficient was determined via the mean-square displacement of Hg atoms in the following way:

$$D = D_{xy} + D_z = \frac{1}{2\Gamma\tau}\left\langle\left[\Delta\mathbf{r}(t)\right]^2\right\rangle_q.$$

Here, $\Gamma = 3$ is the space dimensionality. The angle brackets denote the averaging over q, where q is the number of time intervals required to determine $\left\langle\left[\Delta\mathbf{r}(t)\right]^2\right\rangle$. Five time dependences were averaged, with each of them being calculated within interval τ = 40 ps.

The density profile of a metal film was calculated as follows:

$$\rho(z) = \frac{n(z)\sigma_{\mathrm{Hg}}^3}{\Delta h S_{xy} N_s},$$

where $n(z)$ is the number of Hg atoms in a layer parallel to the graphene plane, σ_{Hg} is the effective diameter of a Hg atom, Δh is the layer width, S_{xy} is the film surface area, and N_s is the number of the tests.

In order to calculate contact angle θ between a droplet (film) surface and graphene, the largest horizontal cross-sectional area of a droplet was divided into three regions: (1) a circle with a constant area, which determines the region of the contact with graphene, (2) a ring comprising the projections of neighbors closest to region (1), and (3) an analogous ring used to reveal the external atoms of the droplet. Mercury atoms closest to the graphene surface were located in regions 2 and 3. Parameters of the procedure used for determining angles θ were selected empirically. The averaging over the sizes of the rings and heights (or the number of selected Hg atoms), at which Hg atoms were located in regions 2 and 3 yielded the average values of the horizontal and vertical coordinates used to find $\tan\theta$. The determination of angle θ required averaging over time as well.

To calculate the stresses developing in graphene, the graphene sheet was divided into surface elements. Atomic stresses $\sigma_{uJ}(l)$ in a surface element with orientation denoted by subscript u and number l for each direction x, y, and z with current subscript J were determined by calculating the kinetic energies of atoms located in this element and projections of forces f_J^i, applied to an l element from the sides of all other atoms as

$$\sigma_{uJ}(l) = \left\langle\sum_i^k \frac{1}{\Omega}\left(m v_J^i v_J^i\right)\right\rangle + \frac{1}{S_l}\left\langle\sum_i^k \left(f_J^i\right)\right\rangle,$$

where k is the number of atoms in element l, Ω is the volume per atom, m is the mass of an atom, v_J^i is the J-projection of the velocity of atom i, and S_l is the area of element l.

Compressing stresses thus determined may have both signs "+" and "–" in accordance with the directions of forces f_J^i. This is the difference between microscopic $\sigma_{uJ}(l)$ and macroscopic $\bar{\sigma}_J < 0$ stresses. The total stresses acting in the graphene plane were determined by adding corresponding elementary stresses as follows:

$$\sigma_{\alpha J} = \sum_{l=1}^{N_l} \sigma_J^{\alpha}(l),$$

where N_l is the number of the surface elements that result from dividing the graphene sheet in a selected direction.

The roughness of the surface (the arithmetical mean deviation of the profile) was calculated as

$$R_a = \frac{1}{N}\sum_{i=1}^{N} |z_i - \bar{z}|,$$

where N is the number of sites (atoms) on the graphene surface, z_i is the level of an ith atom, and $\bar{z}$ is the level of the graphene surface, with the z_i and $\bar{z}$ values being determined at the same time moment.

The total energy obtained at $T = 300$ K for free single-sheet graphene was –7.02 eV, which agreed with the result of the quantum-chemical calculation (–6.98 eV) [31]. The isochore specific heat (28.4 J/(mol K)) calculated for liquid mercury in terms of the MD model at this temperature agrees with the experimental value (26.9 J/(mol K)).

CALCULATION RESULTS

Taking into account the value of the time step, the calculation time, and the addend for the increase in the temperature, it is easy to show that the average rate of the system heating is $\sim 10^{11}$ K/s. Under these conditions of incomplete structural relaxation of the system, it may be superheated. In the case of metals, the superheating is aggravated by the effect of the electron subsystem, which stabilizes the condensed state. Variations accompanying the heating of a mercury film on graphene are illustrated in Fig. 1. The liquid metal film

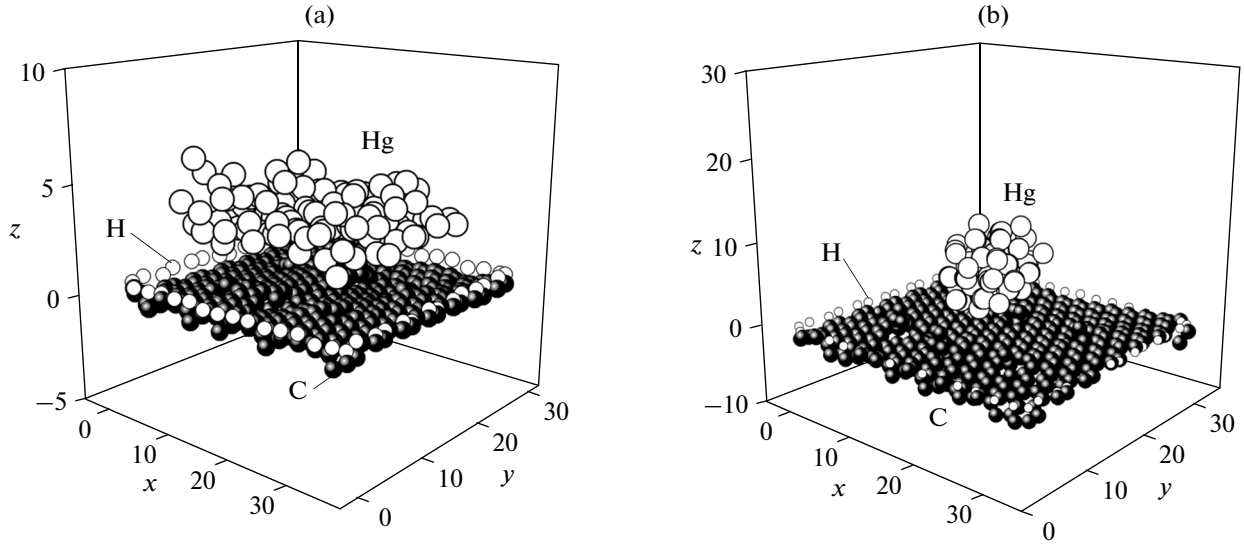

Fig. 1. Configurations of the "Hg film on partly hydrogenated defective graphene" system resulting from stepwise heating at temperatures of (a) 300 and (b) 1100 K. Coordinates of atoms are given in angstroms.

begins to partly separate out of graphene already at $T = 300$ K. This is reflected in the rise of the film edges over graphene and film thickening. The atoms of the central region of the bent Hg film are more strongly bonded to the substrate and have average minimum distance (created by 12–18 Hg atoms) $\overline{r}_{C-Hg}^{min} = 0.28$ nm. At 600 K, the Hg film is completely transformed into a droplet contacting with graphene. In this case, average distance $\overline{r}_{C-Hg}^{min}$ increases to 0.34 nm. A further increase in the temperature leads to a higher rise of the majority of the droplet mass over the graphene surface. For example, at 1100 K, $\overline{r}_{C-Hg}^{min} = 0.47$ nm.

As the Hg film contracts into the droplet, horizontal component D_{xy} of the mobility coefficient of mercury atoms decreases, while vertical component D_z passes through a minimum at 600 K (Fig. 2). The smooth decrease in D_{xy} characterizes the rolling of the film into a dense droplet. The behavior of component D_z indicates that the process of droplet formation ends at $T = 600$ K, and, upon a further increase in the temperature, the vertical mobility is somewhat enhanced because of a slight increase in the distance between the droplet and the graphene surface.

The extent of the transformation of the vibrational spectra of Hg atoms with the temperature increasing from 300 to 1100 K is illustrated in Fig. 3. At $T =$ 300 K, the spectrum of the horizontal vibrations is characterized by strong bursts diminishing with frequency. At 1100 K, the asymptotic of this spectrum remains unchanged, but the intensity of the decreasing peaks drops by six or seven times. The intensity of the vertical vibration spectrum gradually decreases down to disappearance at frequencies $\omega \geq 9.1 \times 10^{12}$ s^{-1} irrespective of the temperature of mercury. However, as the temperature increases, the small-scale vibrations imposed onto the spectrum pattern are smoothed out. The vertical vibration spectrum is wider than the spectrum of horizontal vibrations of Hg atoms.

Vertical (scanned along the oz axis) density profiles $\rho(z)$ of mercury at 300 and 600 K are presented in Fig. 4. The narrow $\rho(z)$ profile measured at $T = 300$ K has two sharp peaks, which suggest a predominantly two-layer arrangement of Hg atoms on graphene. However, at $T = 600$ K, the density profile widens and shifts upward. The low intensity of the $\rho(z)$ spectrum at the edges and the higher density of the intense peaks in the middle of the spectrum characterize the appearance of a spherelike formation, i.e., a droplet with a layered structure, which is evident from the large number of narrow peaks in the $\rho(z)$ spectrum. The very close arrangement of a number of these peaks indicates the irregularity of the formed structure.

The $g(r)$ radial distribution functions (Fig. 5) plotted for the Hg atom nearest to the center of mass of liquid mercury also indicate the formation of a more compact structure at $T = 1100$ K than that at an initial temperature of 300 K. The $g(r)$ function reflects the spherically averaged structure of liquid mercury, including that in the horizontal plane, while the $\rho(z)$ function does not do so. A reduction in the number of peaks in the $g(r)$ function at $T = 1100$ K suggests the formation of an irregular compact structure, in which the distances to the first- and second-order neighbors are estimated to be $r_1 = 0.29$ nm and $r_2 = 0.48$–0.57 nm, respectively. The experimental values of

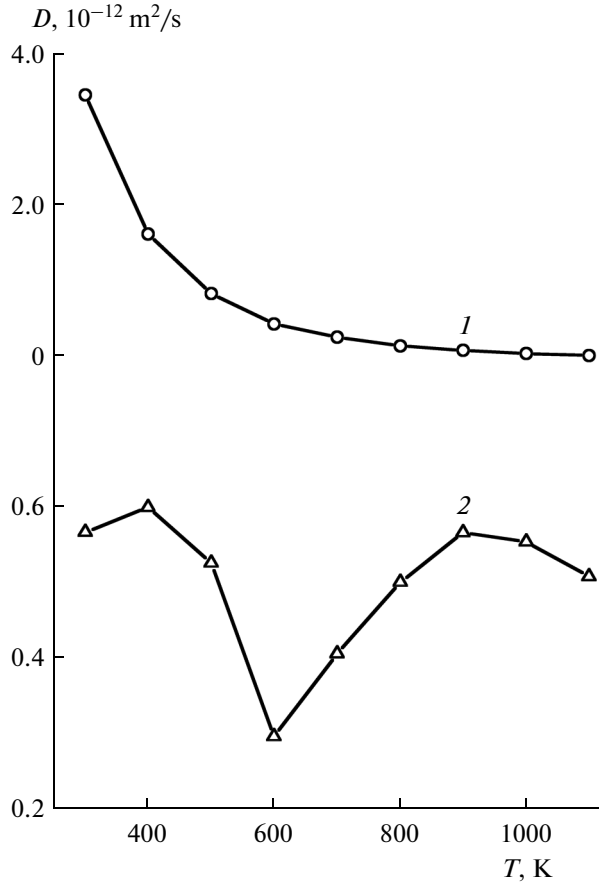

Fig. 2. Temperature dependences of the (*1*) horizontal and (*2*) vertical components of the mobility coefficient for Hg atoms.

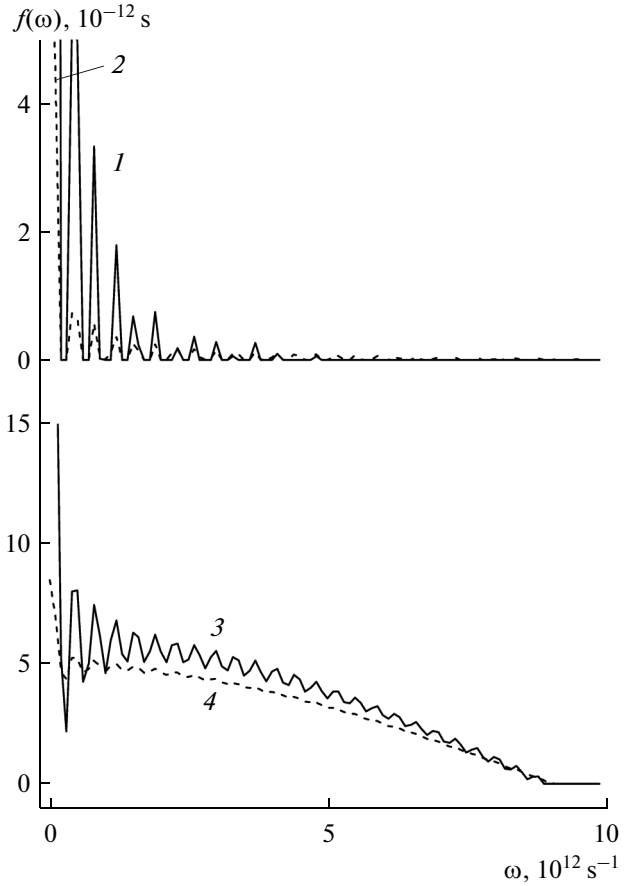

Fig. 3. Frequency dependences of the (*1, 2*) horizontal and (*3, 4*) vertical components of phonon spectrum of liquid mercury on graphene measured at different temperatures: (*1, 3*) 300 and (*2, 4*) 1100 K.

these parameters for liquid mercury at 300 K are $r_1 = 0.31$ nm and $r_2 = 0.59$ nm [32].

Variations in the wettability that accompany mercury film rolling into a droplet are evident from the temperature dependence of calculated contact angle θ (Fig. 6). An initial increase in the θ(T) function (up to $T = 500$ K) is due to the predominance of the influence of film heating over the effect relevant to variations in its morphology. It is known that, as the temperature increases, the blunt contact angle of a droplet becomes closer to the flat angle. In spite of a noticeable rise of the droplet over graphene, which begins from 600 K, its separation from the substrate may only be related to a temperature of 800 K. The calculation at 600 K ends when seven Hg atoms are still located at distances r from graphene shorter than distance $r_{min} = 0.3727$ nm corresponding to the minimum of the LJ potential describing the Hg–C interactions. At 700 K two such cases are observed, while, at $T = 800$ and 900 K, none take place. However, one and two Hg atoms with $r < r_{min}$ arise at $T = 1000$ and 1100 K, respectively. Average angle $\overline{\theta} = 127.1°$, which corresponds to temperatures of 900–1100 K, may be considered to be the contact angle of a 100-atom cluster of Hg on graphene. This angle is noticeably smaller than the contact angle for a macroscopic droplet of mercury on pyrolytic graphite (dashed line in Fig. 6) [5]. This agrees with the common ideas of a reduction in angle θ with a decrease in the droplet radius. The inset of Fig. 6 shows the time dependence of θ at 600 K. It can be seen that angle θ has begun to noticeably decrease by the end of the calculation at this temperature.

A peak at 120°, which indicates the presence of the main elements of the two-dimensional structure, i.e., hexagonal honeycombs, dominates in the angular distribution of the nearest neighbors in graphene at $T = 300$ K (Fig. 7). Additional peaks arise in this distribution due to the high density of the Stone–Wales defects (penta- and heptagonal cells). In spite of the fact that 1100 K is not a high temperature for graphene (its melting temperature is $T_m = 4900$ K), its structure has already suffered from obvious changes. The peak at 120° C has become significantly wider. Moreover, the intensities of peaks at 30°, 90°, and 148° have sub-

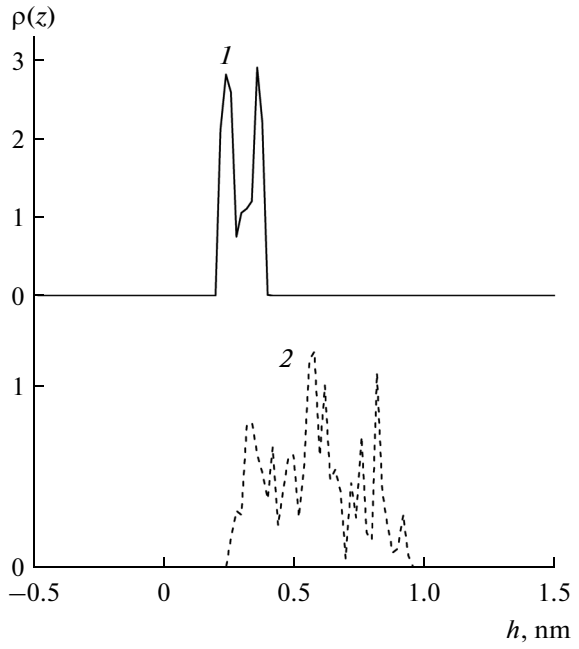

Fig. 4. Vertical density profiles for liquid mercury on graphene at different temperatures: (*1*) 300 and (*2*) 600 K.

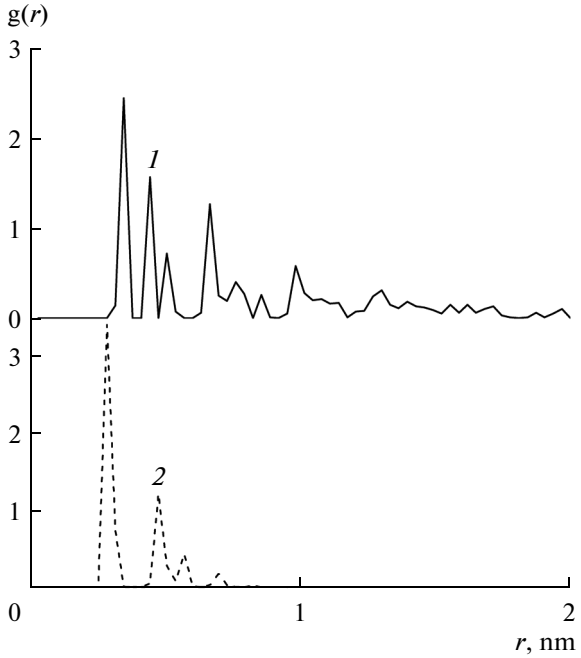

Fig. 5. Radial distribution functions calculated for liquid mercury on graphene at different temperatures: (*1*) 300 and (*2*) 1100 K.

stantially increased. These changes indicate the growth of the defects in the graphene structure at $T =$ 1100 K. Stresses σ_{zx} and σ_{zy}, which characterize the action of the internal horizontal forces in the graphene plane have close values, which weakly vary with an increase in the temperature (Fig. 8). A noticeable difference between these stresses, which is observed at $T =$ 300 K, disappears while approaching a temperature of 500 K. The values of stress σ_{zz}, which characterizes the action of the vertically directed forces, have the same order of magnitude as stresses σ_{zx} and σ_{zy} have. The $\sigma_{zz}(T)$ function comprises two regions of the most rapid variations, i.e., a decrease upon heating to 400 K and an increase upon heating after 1000 K. The lowest values of σ_{zz} are observed in a temperature range of 600–800 K, in which the majority of the droplet mass rises over graphene.

Roughness R_a of graphene saturated with the Stone–Wales defects rapidly increases with temperature (Fig. 9). As a result of vertical bombardment by Xe_{13} clusters with an energy of 30 eV, graphene containing vacancies and coated with a mercury film acquires a roughness, which is close to R_a at 400 K without the bombardment [20]. The strong bond between carbon atoms in graphene is better preserved at a high temperature ($T \geq 1000$ K), when the simulation is performed in terms of the Sch potential than within the framework of the SG potential.

DISCUSSION

Variations in the state of a liquid under a real regime may lead to its superheating, i.e., the existence of the liquid above the boiling temperature upon evaporation. A liquid is superheated as a result of either a rapid heating at a constant pressure or a rapid loss of sealing at a constant temperature. In any case, the liquid enters the region of a nonequilibrium or metastable state, in which its temperature becomes higher than the saturation temperature at normal pressure. The degree of superheating for nonmetal liquids may be as high as several hundred degrees and depends mainly on the rate of heating or reduction in pressure. In the limiting case of complete absence of vapor, very high degrees of superheating may be reached. The superheating is eliminated via an instantaneous change in the phase state, such as explosive boiling up. A high superheating of a liquid is limited by homogeneous nucleation. The ultimate superheating that has been reached for water is (329–333) K [33, 34]. Therewith, a critical nucleus contained nearly 20 molecules [35].

Phase transitions in metal-based systems are distinguished by some specific features. In this case, the electronic and molecular structures of liquid and vaporous phases occurring at equilibrium are greatly different. For example, liquid mercury and cesium at temperatures close to their ordinary melting points are considered to be normal liquid metals having properties typical of a condensed state. Slight changes in the main properties, such as electrical conductivity or magnetic susceptibility as a result of melting show that

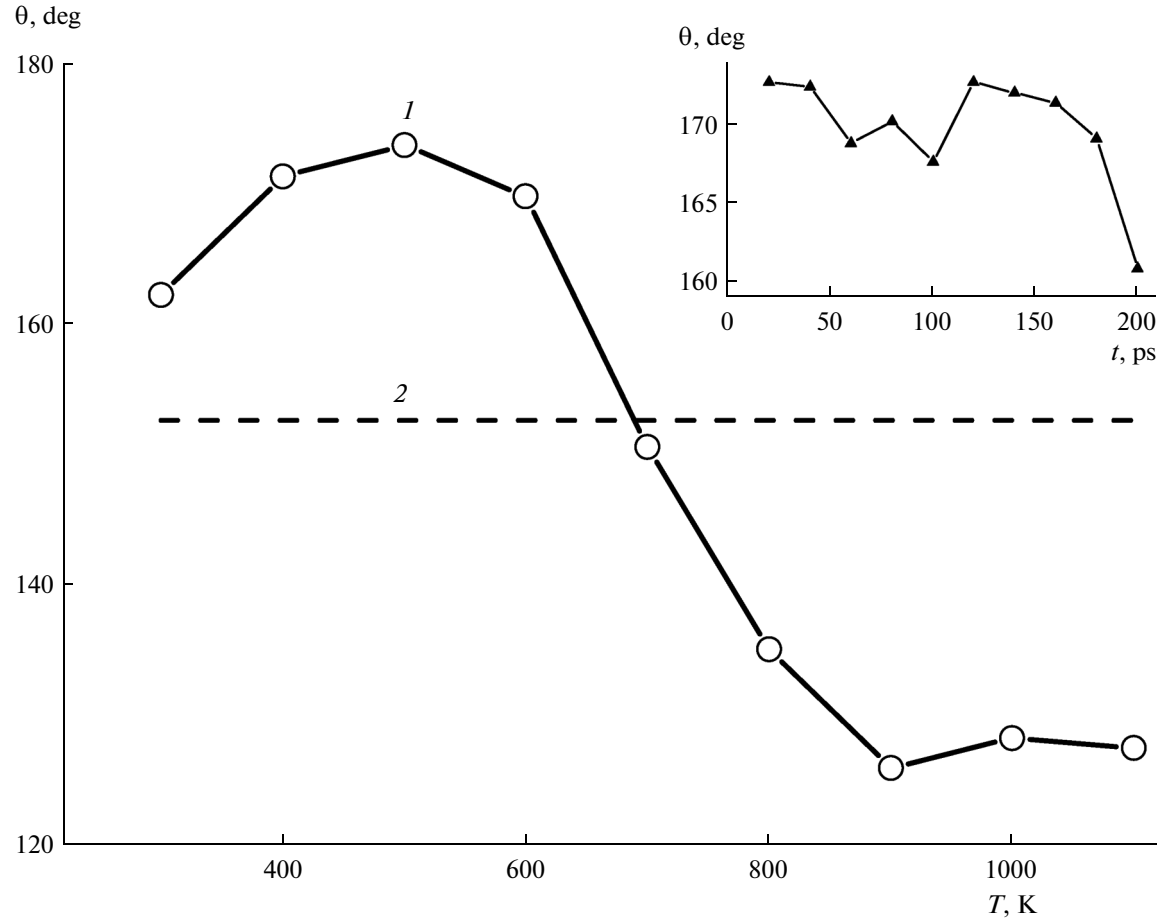

Fig. 6. Temperature dependences of contact angles for (*1*) mercury on graphene and (*2*) macroscopic mercury droplet on pyrolytic graphite [5]. The inset shows the temperature dependence of contact angle for a mercury droplet on graphene at $T = 600$ K.

the electronic structure of the liquid is similar to that of a crystalline solid. This behavior is commonly explained by the fact that the short-range atomic correlations in a small volume are analogous for a liquid and a crystal. In addition, the ion charges in metals are strongly screened by conduction electrons; therefore, the long-range order of ion potentials is of no importance for either a liquid or a solid. The unusual behavior of a metal-based system is evident from the metal–nonmetal transition, which takes place upon the evaporation of a dense liquid, i.e., when it passes into a rarefied vapor, or in the case of liquid expansion upon heating. The low surface free energy of the majority of nonmetal solids excludes their wettability with inert (nonreactive) liquid metals. However, for mercury located on glass, quartz, or sapphire, a prewetting transition is distinctly observed. The existence of the metal–nonmetal transition noticeably affects the thermodynamic, structural, interfacial, and dynamic properties of metals. The conductivity–density dependence for bivalent mercury may be divided into three regions.

Mercury is a polyvalent metal, which is available for studying in the liquid state at low temperatures. The critical point of its vapor is characterized by the following parameters: $T_c = 1751$ K, $p_c = 167.3$ MPa, and $\rho_c = 5.8$ g/cm^3. Mercury has the lowest critical temperature of those known for all liquid metals. This fact is of importance from the point of view of precise measurement of physical properties at high temperatures and pressures.

The experimental data on droplet evaporation on a hot surface indicate the existence of a discontinuity in the dependence of temperature difference $\Delta T = T^i_{vap} - T^i_{liq}$ (i denotes the interface) on vapor pressure p^i_{vap} [36, 37]. At a liquid–vapor interface, the temperature is always higher on the side of the vapor. This is explained by the fact that high-energy molecules are primarily evaporated, while molecules with lower energies remain in the droplet. A reduction in the flux of molecules to the vapor phase is mainly observed at high temperatures—for water, at $T/T_c \approx 0.84$ [38]. The value of the temperature discontinuity for water may be higher than 1400 K [38].

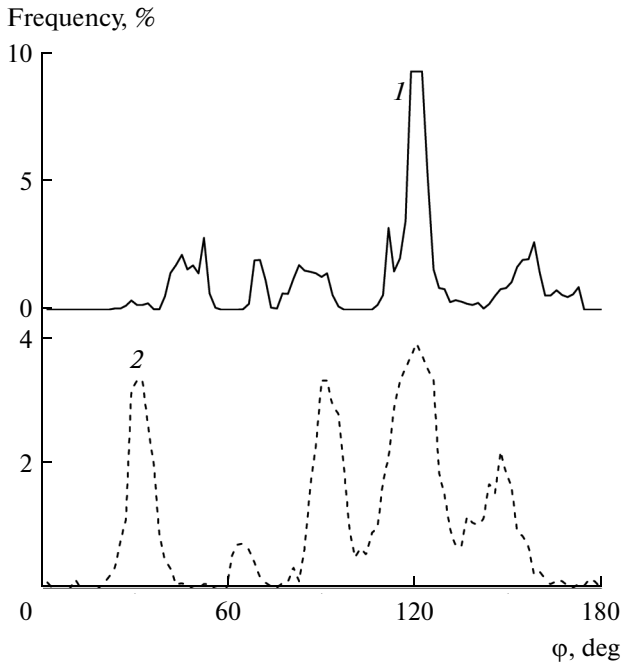

Fig. 7. Angular distributions for nearest neighbors in graphene at a high concentration of Stone–Wales defects and different temperatures: (*1*) 300 and (*2*) 1100 K.

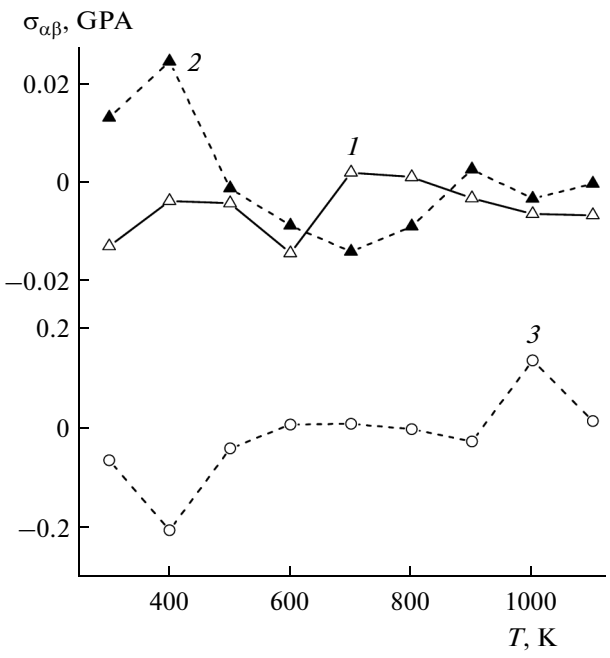

Fig. 8. Temperature dependences of the components of the stress tensor in the plane of a mercury-coated defective graphene sheet: (*1*) σ_{zx}, (*2*) σ_{zy}, and (*3*) σ_{zz}.

Mercury atoms are 11 times heavier than water molecules. Mercury is characterized by another type of interaction. It may be thought that a mercury droplet remains stable at high temperatures because of a reduction in the flux of Hg atoms to the vapor phase; however, the characteristic features of this process differ from the behavior of water.

The high stability of a model mercury droplet may also be explained as follows. The interaction potential between two mercury atoms is, as a rule, considered to be a potential between highly polarizable closed shells, which permit very low migration of electron density from one partner to another; i.e., this potential is, to some extent, similar to a potential function that describes the interaction between atoms of noble gases. We have proven the formation of a mercury droplet on graphene upon rapid heating using a calculation similar to that reported here, but performed in terms of the Sch potential.

In [39], it was noted that the model approximations that use pair interaction potentials to describe the liquid–gas transition for mercury are rough [39]. Experimental gas–liquid coexistence curves may be precisely reproduced, provided that the two-atom curves obtained for potential energy from the former principles are supplemented with the many-particle potential, which describes the associative interaction of an atom with neighboring atoms that altogether form a virtual cluster. The liquid–gas transition for mercury is distinguished by the fact that the local electronic states change from metal to nonmetal ones because of weakened many-particle interactions and decreased average coordination numbers.

According to the calculation in terms of the SG potential, Hg film rolls into a droplet upon heating. By the end of the calculation at 600 K, an almost spherical droplet is formed on graphene, with the droplet

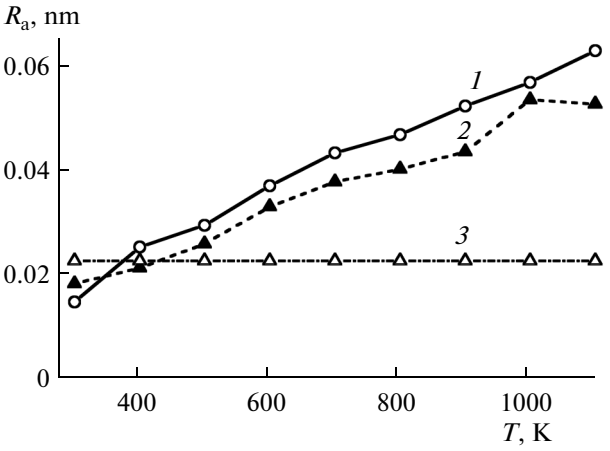

Fig. 9. Temperature dependences of roughness coefficient for mercury-coated graphene with regard to Hg–Hg interactions plotted with the use of different models: (*1*) SG potential and (*2, 3*) Sch potential. Temperature is varied by means of (*1, 2*) heating and (*3*) vertical bombardment by Xe_{13} clusters with an energy of 30 eV.

remaining near the graphene surface even at 1100 K. When the Sch potential function is used, the distance between the droplet and graphene rapidly increases up to a temperature of 1000 K. No significant separation of Hg atoms from the droplet takes place in this case. Most likely, the SG and Sch potentials give an overestimated indirect effect of the electron component on the Hg–Hg interaction, which leads to the high stability of liquid mercury with respect to its vapor.

CONCLUSIONS

Molecular dynamics has been employed to study the stepwise heating of a mercury film on imperfect graphene. A graphene sheet with a high concentration of Stone–Wales defects and hydrogenated edges has been examined. An increase in temperature has been shown to cause gradual rolling of the film into a droplet and a slow movement of the droplet away from graphene. The horizontal component of the mobility coefficient of Hg atoms smoothly decreases in the course of this process, while the vertical component nonmonotonically increases after a reduction reached by a temperature of 600 K. As a whole, the spectra of the horizontal and vertical vibrations of Hg atoms similarly vary with a rise in the temperature; i.e., the small-scale fluctuations of temperature in the spectra are smoothed. The vertical profile of mercury density shifts upward and widens to a size that corresponds to the diameter of the formed liquid metal droplet. The formation of the mercury droplet is accompanied by a reduction in the domain of the radial distribution function and a decrease in the number and intensity of pronounced peaks of the $g(r)$ dependence. An increase in the temperature accelerates the formation of the droplet and decreases the contact angle. In the angular distribution of nearest neighbors, the intensity of the main peak at 120°, which reflects the hexagonal cells, decreases, while intense peaks corresponding to angles of 30°, 90°, and 148° arise. The stresses in the graphene plane that are caused by the horizontal and vertical forces have close magnitudes in the considered temperature range. Graphene roughness rapidly grows with temperature, reaching a maximum value at 1000 K. Hydrogenated graphene edges are not damaged significantly upon heating to high temperatures.

Thus, upon rapid heating, a mercury film on graphene is transformed into a droplet with substantial changes in atomic packing and physical properties.

ACKNOWLEDGMENTS

This work was supported by the Russian Foundation for Basic Research, project no. 13-08-00273.

REFERENCES

1. Lee, C.W., Serre, S.D., Zhao, Y., Lee, S.J., and Hastings, T.W., *J. Air & Waste Manag. Assoc.*, 2008, vol. 58, p. 484.
2. Huggins, F.E., Yap, N., Huffman, G.P., and Senior, C.L., *Fuel Process. Technol.*, 2003, vol. 82, p. 167.
3. Hutson, N.D., Attwood, B.C., and Scheckel, K.G., *Environ. Sci. Technol.*, 2007, vol. 41, p. 1747.
4. Wilcox, J., Sasmaz, E., and Kirchofer, A., *J. Air & Waste Manag. Assoc.*, 2011, vol. 61, p. 418.
5. Awasthi, A., Bhatt, Y.J., and Garg, S.P., *Meas. Sci. Technol.*, 1996, vol. 7, p. 753.
6. Dujardin, E., Ebbesen, T.W., Hiura, H., and Tanigaki, K., *Science* (Washington, D. C.), 1994, vol. 265, p. 1850.
7. Chen, J.Y., Kutana, A., Collier, C.P., and Giapis, K.P., *Science* (Washington, D. C.), 2005, vol. 310, p. 1480.
8. Galashev, A.Y., *Mol. Simul.*, 2010, vol. 36, p. 273.
9. Kutana, A. and Giapis, K., *Phys. Rev. B: Condens. Matter*, 2007, vol. 76, p. 195444.
10. Azamat, J., Khataee, A., and Joo, S.W., *J. Mol. Graph. Model.*, 2014, vol. 53, p. 112.
11. Kim, H.W., Yoon, H.W., Yoon, S.-M., Yoo, B.M., Ahn, B.K., Cho, Y.H., Shin, H.J., Yang, H., Paik, U., Kwon, S., Choi, J.-Y., and Park, H.B., *Science* (Washington, D. C.), 2013, vol. 342, p. 91.
12. Galashev, A.E. and Polukhin, V.A., *Phys. Met. Metallography*, 2014, vol. 115, p. 697.
13. Galashev, A.E. and Galasheva, A.A., *High Energy Chem.*, 2014, vol. 48, p. 112.
14. Galashev, A.E., *Fiz. Mezomekh.*, 2014, vol. 17, no. 1, p. 67.
15. Galashev, A.E. and Polukhin, V.A., *J. Surf. Invest. X-ray, Synchrotron, Neutron Tech.*, 2014, vol. 8, p. 1082.
16. Galashev, A.E. and Rakhmanova, O.R., *High Temp.*, 2014, vol. 52, p. 374.
17. Galashev, A.E., *High Temp.*, 2014, vol. 52, p. 633.
18. Galashev, A.E. and Polukhin, V.A., *Phys. Solid State*, 2013, vol. 55, p. 2368.
19. Galashev, A.E. and Rakhmanova, O.R., *Physics-Uspekhi*, 2014, vol. 57, p. 970.
20. Galashev, A.E. and Galasheva, A.A., *High Energy Chem.*, 2015, vol. 49, p. 117.
21. Zakharchenko, K.V., Fasolino, A., Los, J.H., and Katsnelson, M.I, *J. Phys.: Condens. Matter*, 2011, vol. 23, p. 202202.
22. Tersoff, J., *Phys. Rev. Lett.,* 1988, vol. 61, p. 2879.
23. Stuart, S.J., Tutein, A.V., and Harrison, J.A., *J. Chem. Phys.*, 2000, vol. 112, p. 6472.
24. Munro, L.J. and Johnson, J.K., *J. Chem. Phys.*, 2001, vol. 114, p. 5545.
25. Kutana, A. and Giapis, K.P., *Nano Lett.*, 2006, vol. 6, p. 656.
26. Kim, Y.M. and Kim, S.-C., *J. Korean Phys. Soc.*, 2002, vol. 40, p. 293.
27. Li, F.-Y. and Berry, R.S., *J. Phys. Chem.*, 1995, vol. 99, p. 2459.

28. Lamari, F.D. and Levesque, D., *Carbon*, 2011, vol. 49, p. 5196.
29. Verlet, L., *Phys. Rev.*, 1967, vol. 159, p. 98.
30. Berendsen, H.J.C., Postma, J.P.M., Van Gunsteren, W.F., DiNola, A., and Haak, J.R., *J. Chem. Phys.*, 1984, vol. 81, p. 3684.
31. Davydov, S.Yu., *Phys. Solid State*, 2012, vol. 54, p. 875.
32. Rao, R.V.G. and Murthy, A.K.K., *Phys. Status Solidi B,* 1974, vol. 66, p. 703.
33. Eberhart, J.G. and Pinks, V., *J. Colloid Interface Sci.,* 1985, vol. 7, p. 574.
34. Salla, J.M., Demichela, M., and Casal, J., *J. Loss Prevent. Proc. Ind.*, 2006, vol. 19, p. 690700.
35. Monde, M. and Hasan, M.N., Abstracts of Papers, *Int. Conf. on Mechanical Engineering (ICME2011)*, Dhaka: BUET, 2011, p. KEY-004.
36. Ward, C.A. and Stanga, D., *Phys. Rev. E: Stat. Phys., Plasmas, Fluids, Relat. Interdiscip. Top.*, 2001, vol. 64, p. 051509.
37. McGaugheya, A.J.H. and Ward, C.A., *J. Appl. Phys.*, 2002, vol. 91, p. 6406.
38. Lotfi, A., Vrabec, J., and Fischer, J., *Int. J. Heat Mass Transfer*, 2014, vol. 73, p. 303.
39. Kitamura, H., *J. Phys.: Conf. Ser.*, 2008, vol. 98, p. 052010.

Translated by A. Kirilin